

# Constraining the Evolution of Dark Energy with a Combination of Galaxy Cluster Observables

Sheng Wang<sup>1,2</sup>, Justin Khoury<sup>3</sup>, Zoltán Haiman<sup>4</sup> and Morgan May<sup>1</sup>

<sup>1</sup>*Brookhaven National Laboratory, Upton, NY 11973-5000, USA*

<sup>2</sup>*Department of Physics, Columbia University, New York, NY 10027, USA*

<sup>3</sup>*Institute for Strings, Cosmology and Astroparticle Physics,  
Columbia University, New York, NY 10027, USA*

<sup>4</sup>*Department of Astronomy, Columbia University, New York, NY 10027, USA*

We show that the abundance and redshift distribution ( $dN/dz$ ) of galaxy clusters in future high-yield cluster surveys, combined with the spatial power spectrum ( $P_c(k)$ ) of the same clusters, can place significant constraints on the evolution of the dark energy equation of state,  $w = w(a)$ . We evaluate the expected errors on  $w_a = -dw/da$  and other cosmological parameters using a Fisher matrix approach, and simultaneously including cluster structure evolution parameters in our analysis. We study three different types of forthcoming surveys that will identify clusters based on their X-ray emission (such as DUO, the Dark Universe Observatory), their Sunyaev-Zel'dovich (SZ) decrement (such as SPT, the South Pole Telescope), or their weak lensing (WL) shear (such as LSST, the Large Synoptic Survey Telescope). We find that combining the cluster abundance and power spectrum significantly enhances constraints from either method alone. We show that the weak-lensing survey can deliver a constraint as tight as  $\Delta w_a \sim 0.1$  on the evolution of the dark energy equation of state, and that the X-ray and SZ surveys each yield  $\Delta w_a \sim 0.4$  separately, or  $\Delta w_a \sim 0.2$  when these two surveys are combined. For the X-ray and SZ surveys, constraints on dark energy parameters are improved by a factor of two by combining the cluster data with cosmic microwave background (CMB) anisotropy measurements by Planck, but degrade by a factor of two if the survey is required to solve simultaneously for cosmological and cluster structure evolution parameters. The constraint on  $w_a$  from the weak lensing survey is improved by  $\sim 25\%$  with the addition of Planck data.

## I. INTRODUCTION

It has long been realized that clusters of galaxies provide a useful probe of fundamental cosmological parameters. The formation of the massive dark matter potential wells is dictated by simple gravitational physics, and the abundance and redshift distribution of clusters ( $dN/dz$ ) should be determined by the geometry of the universe and the power spectrum of initial density fluctuations. Early studies of nearby clusters used this relation to constrain the amplitude  $\sigma_8$  of the power spectrum (e.g., [1, 2]). Subsequent works (e.g., [3, 4, 5]) have shown that the redshift-evolution of the observed cluster abundance places useful constraints on the matter density parameter  $\Omega_m$ .

The next generation of surveys, utilizing the Sunyaev-Zel'dovich effect (SZE), X-ray flux, or weak lensing signatures to identify galaxy clusters, will be able to deliver large catalogs, containing many thousands of clusters, with complementary selection criteria. Such forthcoming datasets have rekindled a strong theoretical and experimental interest in galaxy clusters. In particular, Wang & Steinhardt [6] first argued that the cluster abundance can be used to probe the properties of dark energy, and Haiman, Mohr & Holder [7] showed that a survey with several thousand clusters can yield precise statistical constraints on both its density ( $\Omega_{\text{DE}}$ ) and its equation of state ( $w \equiv P/\rho$ ). Several subsequent recent works have focused on various aspects of extracting cosmological parameters from high-yield, future surveys, such as the sta-

tistical constraints available on curvature  $\Omega_k$  [8]; assessing the impact of sample variance [9] and other uncertainties [10] on parameter estimates; and controlling such uncertainties by utilizing information from the shape of the cluster mass function  $dN/dM$  [11]. Closest to the subject of the present paper, Weller *et al.* [12] and Weller & Battye [13] considered constraints on the time evolution of the dark energy equation of state in forthcoming SZE cluster surveys.

Recent studies have elucidated the additional cosmological information available from the spatial distribution of galaxy clusters through a measurement of their three-dimensional power spectrum  $P_c(k)$  [14] (see [15] for a more general treatment of extracting cosmological information from redshift surveys). The power spectrum contains cosmological information from the intrinsic shape of the transfer function [16] and from baryon features [17, 18, 19]. The existing sample of  $\sim 400$  nearby clusters in the REFLEX survey has already been used to derive their power spectrum; combined with the number counts, this has yielded constraints on  $\sigma_8$  and  $\Omega_m$  that are consistent with other recent determinations [20].

Most importantly, the cluster abundance and power spectrum can provide two independent powerful probes of cosmological parameters from a single dataset. The dependence of  $dN/dz$  and  $P_c(k)$  on the cosmological parameters are different. Combining the two pieces of information can therefore break degeneracies present in either method alone, and yield tighter statistical constraints. Furthermore, this can be used to significantly reduce systematic errors arising from the mass-observable rela-

tion, making cluster surveys “self-calibrating” [21]. This self-calibration is especially strong when the abundance and power spectrum information is combined with even a modest follow-up mass calibration program [22].

In this paper, we return to the question of constraining the time-evolution of the dark energy equation of state. Specifically, we ask the question: *can improved constraints be obtained on the time-evolution of  $w = w(z)$  when the cluster counts and power spectrum are combined?* We quantify the statistical constraints expected to be available from future samples of  $\gtrsim 10,000$  galaxy clusters.

We study constraints from three different types of forthcoming cluster surveys. The proposed DUO (*Dark Universe Observatory*) [23] X-ray survey will be performed by an Earth-orbiting satellite consisting of seven telescopes that take a wide survey of the sky in soft X-ray bands. The SPT-like (*South Pole Telescope*) [24] SZE survey will be performed by an 8-meter precision submillimeter-wave telescope detecting distant galaxy clusters by their Sunyaev-Zel'dovich decrement. The LSST-like (*Large Synoptic Survey Telescope*) [25] survey will be performed by a ground-based telescope detecting clusters by their weak lensing shear signature on background galaxies.

The most important differences between the present paper and earlier works that have addressed the time-evolution of the equation of state [12, 13] are that here (i) we simultaneously include the abundance and power spectrum in our analysis; (ii) in addition to the cosmological parameters, we simultaneously include several parameters that describe cluster structure and evolution; and (iii) we study three different types of forthcoming surveys. We also chose a different fiducial model for our analysis (one close to the standard “concordance” cosmology). Our calculational method, based on Fisher matrices, is, on the other hand, only a simple approximation to the Monte-Carlo likelihood analysis performed in [12, 13].

This paper is organized as follows. In §II, we describe our basic calculational methods. In §III, we present our results for different future cluster surveys. In §IV, we critically discuss our results, including their uncertainties, and summarize the implications of this work.

## II. CALCULATIONAL METHOD

### A. Simulating Cluster Surveys

We follow the standard approach, and identify galaxy clusters with dark matter halos. The differential comoving number density of clusters is given by Jenkins *et al.* [26]

$$\frac{dn}{dM}(z, M) = 0.301 \frac{\rho_m}{M} \frac{d \ln \sigma^{-1}(M, z)}{dM} \times \exp[-|\ln \sigma^{-1}(M, z) + 0.64|^{3.82}], \quad (1)$$

where  $\sigma^2(M, z)$  is the variance of the linear density field at redshift  $z$ , smoothed with a spherical top-hat filter which would enclose mass  $M$  at the mean present-day matter density  $\rho_m$  [56]. The Jenkins *et al.* mass function was derived from numerical simulations, and its self-similar form is demonstrated to be accurate to within  $\sim 15\%$  in three widely separated cosmologies (although see [27] who find a more significant cosmology-dependence of the mass function). Jenkins *et al.* identify simulated clusters using  $M_{180}$ , the mass enclosed within a spherical overdensity of 180 with respect to the *mean* matter density. However, it is customary to define the relation between X-ray or SZE flux and halo mass  $M_{200}$ , defined as the cluster mass enclosed within a sphere with mean interior overdensity of 200 relative to the *critical* density. To combine this relation with the mass function in Eq. (1), we convert  $M_{200}$  to  $M_{180}$  assuming that the halo density profile is described by the NFW model with a concentration parameter of  $c_{\text{nfw}} = 5$  [28].

The spatial distribution of clusters is assumed to follow the spatial distribution of the dark matter halos and is specified by the cluster power spectrum  $P_c(k)$ . We follow Hu & Haiman [14] and obtain  $P_c(k)$  from the underlying mass power spectrum,  $P(k)$ , modified by redshift-space distortions [29]

$$P_c(k_\perp, k_\parallel) = \left[ 1 + \beta \left( \frac{k_\parallel}{k} \right)^2 \right]^2 b^2 P(k), \quad (2)$$

$$k^2 = k_\perp^2 + k_\parallel^2, \quad (3)$$

where  $k_\perp$  and  $k_\parallel$  are the wavenumbers of the sinusoidal fluctuation modes transverse and parallel to the line of sight, respectively. The redshift-distortion parameter  $\beta$  is defined by [29]

$$\beta = \frac{1}{b} \frac{d \ln D_{\text{grow}}}{d \ln a}, \quad (4)$$

where  $D_{\text{grow}}$  is the linear growth rate, and  $a$  is the expansion factor normalized to unity today. The parameter  $b$  in Eqs. (2) and (4) represents the linear bias averaged over all halos at redshift  $z$ :

$$b(z) = \int_{M_{\min}(z)}^{\infty} \frac{dn(M, z)}{dM} b(M) dM \left[ \int_{M_{\min}(z)}^{\infty} \frac{dn}{dM} dM \right]^{-1}, \quad (5)$$

where  $M_{\min}(z)$  is the mass of the smallest detectable cluster, which depends on the type of survey as discussed in §II.D. The bias parameter of halos of a fixed mass  $M$ ,  $b(M)$ , is assumed to be scale independent and given by

$$b(M) = 1 + \frac{a \delta_c^2 / \sigma^2 - 1}{\delta_c} + \frac{2p/\delta_c}{1 + (a \delta_c^2 / \sigma^2)^p}, \quad (6)$$

with  $a = 0.75$  and  $p = 0.3$  providing the best fits to the clustering measured in cosmological simulations [30]. Finally,  $\delta_c$  represents the threshold linear overdensity corresponding to spherical collapse, whose value is  $\delta_c = 1.686$

in an Einstein–de Sitter universe. We keep it fixed throughout the calculation, as it was shown to be only weakly dependent on cosmology and redshift in other models [6].

## B. Fisher Matrix Technique

The Fisher matrix formalism allows a forecasting of the ability of a given survey to constrain cosmological parameters [31]. It gives a lower bound to the statistical uncertainty of each model parameter that is to be fit by future data. The well-known advantages of the Fisher matrix technique are that (i) it allows a quick estimate of errors in a multi-dimensional parameter space, since the likelihood functions do not have to be evaluated at each point of the multi-dimensional grid, and (ii) constraints from independent data sets or methods can be easily combined by simply summing the individual Fisher matrices.

The Fisher matrix is defined as

$$F_{ij} = \left\langle \frac{\partial^2 \mathcal{L}}{\partial p_i \partial p_j} \right\rangle, \quad (7)$$

where  $\mathcal{L} = -\ln L$  is the log-likelihood function, and where  $p_i$ 's are the various model parameters which, in our case, include both cosmological parameters and parameters describing cluster structure and evolution. The inverse  $(F^{-1})_{ij}$  gives the best attainable covariance matrix, regardless of any specific method used to estimate the parameters from the data [31]. In particular, the best statistical uncertainty attainable on any individual parameter  $p_i$ , after marginalization over all other parameters, is  $(F^{-1})_{ii}^{1/2}$ .

We construct the Fisher matrix for the redshift distribution of the number density of galaxy clusters as [8]

$$F_{\mu\nu}^{\text{counts}} = \sum_i \frac{\partial N_i}{\partial p_\mu} \frac{\partial N_i}{\partial p_\nu} \frac{1}{N_i}, \quad (8)$$

where

$$N_i = \Delta\Omega \Delta z \frac{d^2V}{dzd\Omega}(z_i) \int_{M_{\min}(z_i)}^{\infty} \frac{dn(M, z_i)}{dM} dM \quad (9)$$

is the number of clusters above the detection threshold in each redshift bin  $i$  centered at  $z_i$ . In Eq. (9),  $\Delta\Omega$  is the solid angle covered by a survey,  $d^2V/dzd\Omega$  is the comoving volume element, and  $dn/dM$  is the cluster mass function (see Eq. (1)). We sum over redshift bins of size  $\Delta z = 0.05$ , between  $z_{\min} = 0$  and  $z_{\max} = 2.0$  for the DUO X-ray survey and the SPT-like SZE survey, and between  $z_{\min} = 0.1$  and  $z_{\max} = 1.4$  for the LSST-like survey, although accurate redshifts are not required for the  $dN/dz$  test.

TABLE I: Parameters for the Planck Survey.

Frequency (GHz)	100	143	217
$\theta_c$ (arcmin)	10.7	8.0	5.5
$\sigma_{c,T}$ ( $\mu\text{K}$ )	5.4	6.0	13.1
$\sigma_{c,E}$ ( $\mu\text{K}$ )	--	11.4	26.7
$\ell_c$	757	1012	1472

We construct the Fisher matrix for the redshift–space power spectrum as [14]

$$F_{\mu\nu}^{\text{power}} = \sum_{i,j} \frac{\partial \ln(k_\perp^2 k_{\parallel} P_c)_{ij}}{\partial p_\mu} \frac{\partial \ln(k_\perp^2 k_{\parallel} P_c)_{ij}}{\partial p_\nu} \frac{(V_k V_{\text{eff}})_{ij}}{2}, \quad (10)$$

where  $P_c(k)$  is the cluster power spectrum. The two-dimensional  $k$ –space cells and the set of redshift bins are labeled by  $i$  and  $j$ , respectively. The factor of  $(V_k V_{\text{eff}}/2)^{-1}$  estimates the uncertainty  $(\Delta P_c/P_c)^2$  in the measured power spectrum, including the effects of shot noise and cosmic variance [32]. Here  $V_{\text{eff}}$  is the effective volume probed by the survey

$$V_{\text{eff}}(k) = \int dV_s \left[ \frac{\bar{n}(z_j) P_c(k)}{1 + \bar{n}(z_j) P_c(k)} \right]^2, \quad (11)$$

where  $\bar{n}$  is the expected average number density, and  $V_k$  is the cylindrical volume factor in  $k$ –space:

$$V_k = \frac{2\pi \Delta(k_\perp^2) \Delta k_{\parallel}}{(2\pi)^3}. \quad (12)$$

We sum over  $29^2$  linearly spaced  $k$  cells from  $k_{\perp,\parallel} = 0.005$  to  $0.15 \text{ Mpc}^{-1}$ , thus defining a cylinder in three-dimensional  $k$ –space. We sum over redshift bins of size  $\Delta z = 0.2$ , between  $z_{\min} = 0$  and  $z_{\max} = 2.0$  for the DUO–like survey and the SPT–like survey, and between  $z_{\min} = 0.1$  and  $z_{\max} = 1.4$  for the LSST–like survey. The choice of this relatively wide redshift bin size is dictated by the need to have a sufficient number of clusters in each bin for an accurate determination of the power spectrum ( $N \gtrsim 1,000$ ), as well as a wide enough  $\Delta z$  that includes radial modes with  $k_{\perp,\parallel} \approx 0.005 \text{ Mpc}^{-1}$ .

Finally, in addition to the constraints from clusters considered here, we construct the Fisher matrix that can be used to forecast cosmological parameter errors from the temperature and polarization anisotropy of the cosmic microwave background (CMB). We have in mind a near–future survey such as Planck [33] that will measure temperature and E–mode polarization auto–correlation (respectively, TT and EE), as well as temperature–polarization cross–correlation (TE). We neglect B–mode polarization. The full CMB Fisher matrix is then given by [34, 35]

$$F_{\mu\nu}^{\text{cmb}} = \sum_{\ell} \sum_{X,Y} \frac{\partial C_{X,\ell}}{\partial p_\mu} \text{Cov}^{-1}(C_{X,\ell}, C_{Y,\ell}) \frac{\partial C_{Y,\ell}}{\partial p_\nu}, \quad (13)$$

where  $X, Y$  run over  $TT$ ,  $EE$  and  $TE$  correlations. The covariance matrix,  $\text{Cov}(C_{X,\ell}, C_{Y,\ell})$ , has elements

$$\begin{aligned}\text{Cov}(C_{TT,\ell}, C_{TT,\ell}) &= \frac{2}{(2\ell+1)f_{\text{sky}}}(C_{TT,\ell} + B_{T,\ell}^{-2})^2 \\ \text{Cov}(C_{EE,\ell}, C_{EE,\ell}) &= \frac{2}{(2\ell+1)f_{\text{sky}}}(C_{EE,\ell} + B_{E,\ell}^{-2})^2 \\ \text{Cov}(C_{TE,\ell}, C_{TE,\ell}) &= \frac{1}{(2\ell+1)f_{\text{sky}}}[C_{TE,\ell}^2 + \\ &\quad (C_{TT,\ell} + B_{T,\ell}^{-2})(C_{EE,\ell} + B_{E,\ell}^{-2})] \\ \text{Cov}(C_{EE,\ell}, C_{TE,\ell}) &= \frac{2}{(2\ell+1)f_{\text{sky}}}C_{TE,\ell}(C_{EE,\ell} + B_{E,\ell}^{-2}) \\ \text{Cov}(C_{TT,\ell}, C_{TE,\ell}) &= \frac{2}{(2\ell+1)f_{\text{sky}}}C_{TE,\ell}(C_{TT,\ell} + B_{T,\ell}^{-2}) \\ \text{Cov}(C_{TT,\ell}, C_{EE,\ell}) &= \frac{2}{(2\ell+1)f_{\text{sky}}}C_{TE,\ell}^2, \end{aligned}\quad (14)$$

where  $f_{\text{sky}}$  is the fraction of the sky covered. The  $B_{T,\ell}$ 's and  $B_{E,\ell}$ 's account for experimental noise for temperature and polarization measurements, respectively, and are given by [36]

$$B_{\ell}^2 = \sum_c (\sigma_c \theta_c)^{-2} e^{-\ell(\ell+1)/\ell_c^2}, \quad (15)$$

where the sum is over the different frequency channels denoted by  $c$ ,  $\sigma_c$  is the sensitivity,  $\theta_c$  is the beam width, and  $\ell_c \equiv 2\sqrt{2 \ln 2}/\theta_c$  is the corresponding “cut-off” multipole. Equation 15 assumes that different channels provide independent constraints. We follow previous theoretical “error forecast” work in adopting this assumption; however, we note that this implicitly assumes that all foregrounds were perfectly removed from the temperature and polarization maps. In reality, imperfect removal of foregrounds will induce correlations among the channels, which will have to be taken into account in a refined analysis. Modeling foregrounds and the expected precision with which they can be removed is beyond the scope of the present paper.

In this paper we focus on the Planck survey for concreteness. This survey will measure temperature and polarization anisotropy in three frequency bands, namely 100, 143 and 217 GHz, with fractional sky coverage of  $f_{\text{sky}} \approx 0.8$ . The parameters for this experiment are listed in Table I (taken from [36]). The various  $C_{\ell}$ 's are calculated up to  $\ell_{\text{max}} = 2,000$ , as appropriate for Planck, using KINKFAST [37], a modified version of CMBFAST [38] tailored for time-varying  $w$ .

### C. Fiducial Cosmology

The Fisher matrix formalism estimates how well a survey can distinguish a fiducial model of the universe from other models. The results depend on the fiducial model itself. Throughout the paper, we take a 7-dimensional parameterization of a spatially-flat ( $\Omega_k = 0$ ), cold dark

matter (CDM) cosmological model, dominated by a cosmological constant ( $\Lambda$ ). The sensitivity of our results to the choice of the fiducial parameters is discussed in § IV below. The parameters are adopted from recent measurements by the *Wilkinson Microwave Anisotropy Probe (WMAP)*, as summarized in Table 1 of [39]: baryon density  $\Omega_b h^2 = 0.024$ , matter density  $\Omega_m h^2 = 0.14$ , dark energy density in units of the critical density  $\Omega_{\text{DE}} = 0.73$  (or Hubble constant  $H_0 = 100h \text{ km s}^{-1} \text{ Mpc}^{-1}$  with  $h = 0.72$ ), with present-day normalization  $\sigma_8 = 0.9$  and scalar power-law slope  $n_s = 1$  of the primordial power spectrum. Following Linder [19], we parameterize the evolving dark energy equation of state as

$$w(z) = w_0 + w_a(1 - a) = w_0 + w_a \frac{z}{1+z}, \quad (16)$$

with values in our fiducial model chosen to be  $w_0 = -1$  and  $w_a = 0$ . An alternative parameterization sometimes used in the literature is  $w(z) = w_0 + w_z z$ . The errors we obtain here on  $w_a$  should be divided by approximately a factor of two to obtain the corresponding errors on  $w_z$ . This follows from Taylor-expanding Eq. (16) about  $z = 1/2$ , which is approximately where the sensitivity of cluster surveys peak.

### D. Survey Parameters

To determine the detection mass limit  $M_{\min}(z)$  in Eq. (1), a mass–observable relation is needed. We consider three surveys for our analysis, a flux limited X-ray survey, such as DUO, an SZE survey that is similar to the one to be carried out with the South Pole Telescope, and a weak lensing survey that is similar to that planned for the LSST. For the X-ray and SZE surveys, we impose a minimum mass of  $10^{14}h^{-1}M_{\odot}$  (if  $M_{\min}(z)$  as computed below turns out to be less than  $10^{14}h^{-1}M_{\odot}$ ) since less massive halos correspond to small clusters or groups and are likely to depart from the scaling relations adopted here. We do not impose this lower bound for the weak lensing survey since, in principle, the dark matter halos of low-mass clusters or groups should still produce shear signals with a well-defined mass–shear relation.

For the *DUO-like X-ray survey*, we adopt a bolometric flux–mass relation of the form:

$$f_x(z)4\pi d_L^2 = A_x M_{200}^{\beta_x} E^2(z)(1+z)^{\gamma_x}, \quad (17)$$

where  $f_x$  in units of  $\text{erg s}^{-1} \text{ cm}^{-2}$  is the bolometric flux limit,  $d_L$  in units of Mpc is the luminosity distance,  $M_{200}$  is the mass of the cluster, and  $H(z) = H_0 E(z)$  is the Hubble parameter at redshift  $z$ . Following Majumdar & Mohr [21], we adopt  $\log_{10}(A_x) = -4.159$ ,  $\beta_x = 1.807$ , and  $\gamma_x = 0$  as fiducial values. We model the DUO observations as a combination of a “wide” survey, covering a sky area of  $\Delta\Omega = 6,000 \text{ deg}^2$  with a bolometric flux limit of  $f_x > 1.75 \times 10^{-14} \text{ erg s}^{-1} \text{ cm}^{-2}$  (corresponding to  $f_x > 7 \times 10^{-14} \text{ erg s}^{-1} \text{ cm}^{-2}$  in the 0.5 : 10 keV band);

and a “deep” survey, spanning  $\Delta\Omega = 150 \text{ deg}^2$  with a bolometric flux limit of  $f_x > 2.25 \times 10^{-14} \text{ erg s}^{-1} \text{ cm}^{-2}$  ( $f_x > 9 \times 10^{-15} \text{ erg s}^{-1} \text{ cm}^{-2}$  in the  $0.5 : 10 \text{ keV}$  band). With these parameters, for our fiducial cosmological model, the wide survey yields  $\sim 10,000$  clusters while the deep survey yields  $\sim 1,500$  clusters. These numbers are consistent with the existing data on the  $\log N - \log S$  relation for clusters in soft X-ray bands [40] and also with independent estimates for the total number of clusters expected to be detected by DUO [21].

For an *SPT-like SZE survey*, we adopt an SZE flux-mass relation:

$$f_{sz}(z)d_A^2 = f(\nu)f_{\text{ICM}}A_{sz}M_{200}^{\beta_{sz}}E^{2/3}(z)(1+z)^{\gamma_{sz}}, \quad (18)$$

where  $f_{sz}$  in units of mJy is the observed flux decrement,  $d_A$  in units of Mpc is the angular diameter distance,  $f(\nu)$  is the frequency dependence of the SZE distortion, and  $f_{\text{ICM}}$  is the mass fraction of the intra-cluster medium. We model the SPT-like SZE survey as a flux-limited survey with  $f_{sz} > 5 \text{ mJy}$  at 150 GHz. While this is an oversimplification, the threshold value approximately represents the total flux decrement of the smallest cluster that can be detected at  $5\sigma$  significance with SPT. [57] We also adopt the fiducial parameters  $\log_{10}(A_{sz}) = 8.9$ ,  $\beta_{sz} = 1.68$ ,  $\gamma_{sz} = 0$ , and covering  $\Delta\Omega = 4,000 \text{ deg}^2$ . We also assume  $f_{\text{ICM}} = 0.12$ . With these parameters, for our fiducial cosmological model, this survey yields  $\sim 20,000$  clusters.

Finally, for the *LSST-like WL survey*, we follow Hamana *et al.* [41] to find a relation between the dimensionless shear and halo mass, given by

$$\kappa_G = \alpha(\theta_G) \left[ \frac{M_{\text{vir}}/(\pi r_s^2)}{\Sigma_{cr}} \right]. \quad (19)$$

Here  $\kappa_G$  is the average shear within a Gaussian filter of angular size  $\theta_G$ ;  $M_{\text{vir}}$  and  $r_s$  are the mass and scale radius of a cluster with an NFW density profile ( $r_s = r_{\text{vir}}/c_{\text{nfw}}$ );  $z_l$  is the redshift of the cluster; and  $d_A$  is the angular diameter distance to the cluster. The coefficient  $\alpha$  is given by

$$\alpha = \frac{\int_0^\infty dx (x/x_G^2) \exp(-x^2/x_G^2) f(x)}{\log(1+c_{\text{nfw}}) - c_{\text{nfw}}/(1+c_{\text{nfw}})}, \quad (20)$$

where  $x = \phi/\theta_s$  a dimensionless angular coordinate, and  $x_G \equiv \theta_G/\theta_s$  corresponds to the smoothing scale, with  $\theta_s = r_s/d_A(z_l)$  denoting the angular scale radius. The dimensionless surface density profile  $f(x)$  is given by equation (7) in Hamana *et al.* [41]. Finally, the mean inverse critical surface mass density is given by

$$\Sigma_{cr}^{-1} = \frac{4\pi G}{c^2} a(z_l) \chi(z_l) \frac{\int_{z_l}^\infty dz dn/dz (1 - \chi(z_l)/\chi(z))}{\int_0^\infty dz dn/dz}, \quad (21)$$

where  $a$  is the scale factor and  $\chi$  denotes the comoving radial distance (valid for the flat universe with  $\Omega_k = 0$  we are assuming).

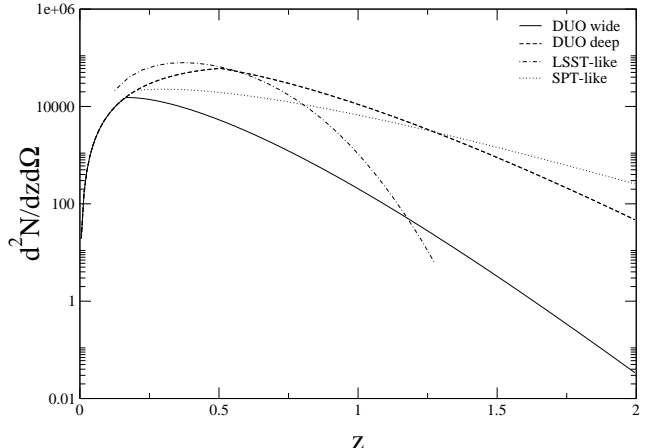


FIG. 1: Expected number of clusters per redshift per unit solid angle for the fiducial cosmology.

We model the LSST-like survey to have a constant detection threshold of  $\kappa_G = 4.5\sigma_{\text{noise}}$  [42]. The noise is given by the ratio of the mean ellipticity dispersion ( $\sigma_\epsilon$ ) of galaxies and the total number of background galaxies contained within a smoothing aperture  $\theta_G$  [43],  $\sigma_{\text{noise}}^2 = \sigma_\epsilon^2/(4\pi\theta_G^2 n_g)$ . We adopt  $\sigma_\epsilon = 0.3$  and a number density of background galaxies  $n_g = 65 \text{ arcmin}^{-2}$  [44], and the angular smoothing scale  $\theta_G = 1 \text{ arcmin}$ , which corresponds to optimal S/N for the range of cluster masses and redshifts we considered. We take the survey to cover  $\Delta\Omega = 18,000 \text{ deg}^2$  and to extend over the cluster redshift range  $0.1 \leq z \leq 1.4$ . This yields  $\sim 200,000$  clusters for our fiducial cosmology.

Evidently, the various surveys considered here span different redshift range, sky coverage and sensitivity. It is therefore useful to compare the expected number of clusters per redshift and unit solid angle for each survey for our fiducial cosmology. This is shown in Fig. 1. We see that the SPT-like survey is the most sensitive probe at high redshift, a consequence of the fact that the mass limit for SZE surveys is nearly redshift-independent. In comparison, the DUO X-ray and LSST-like surveys drop more sharply with redshift. Note that the fixed “mass floor” of  $10^{14}h^{-1}M_\odot$  determines the number of clusters at  $z < 0.2, 0.25, 0.5$  for DUO wide, SPT-like and DUO deep, respectively. In comparison, the LSST-like counts are dominated by small clusters or groups with  $M \leq 10^{14}h^{-1}M_\odot$ .

### III. RESULTS

Before discussing our results for the cluster surveys, we first summarize constraints from the CMB alone. Our projections for the Planck satellite, using the seven-parameter Fisher matrix, are listed in Table II and are consistent with well-known previous forecasts [35, 45, 46]. This table shows the power of the CMB in constraining the matter and baryon density,  $\Omega_m h^2$  and  $\Omega_b h^2$ ,

TABLE II: Estimated Cosmological Parameter Constraints from Planck.

Planck Survey	
$\Delta\Omega_{\text{DE}}$	0.035
$\Delta\Omega_m h^2$	0.0012
$\Delta\sigma_8$	0.041
$\Delta w_0$	0.32
$\Delta w_a$	1.0
$\Delta\Omega_b h^2$	0.00014
$\Delta n_s$	0.0035

TABLE III: Estimated Cosmological Parameter Constraints from DUO. The  $dN/dz$  column includes priors from WMAP:  $\Delta\Omega_b h^2 = 0.0010$ , and  $\Delta n_s = 0.040$ .

Survey and Parameter Constraints	$dN/dz$	$P_c(k)$
<b>DUO Wide (6,000 deg<sup>2</sup>)</b>		
$\Delta\Omega_{\text{DE}}$	0.14	0.037
$\Delta\Omega_m h^2$	0.25	0.096
$\Delta\sigma_8$	0.16	0.10
$\Delta w_0$	0.16	0.59
$\Delta w_a$	0.92	3.2
$\Delta\Omega_b h^2$	0.0010	0.023
$\Delta n_s$	0.040	0.18
<b>DUO Deep (150 deg<sup>2</sup>)</b>		
$\Delta\Omega_{\text{DE}}$	0.097	0.11
$\Delta\Omega_m h^2$	0.33	0.25
$\Delta\sigma_8$	0.040	0.25
$\Delta w_0$	0.29	0.78
$\Delta w_a$	2.5	3.7
$\Delta\Omega_b h^2$	0.0010	0.059
$\Delta n_s$	0.040	0.49

respectively, as well as the spectral tilt,  $n_s$ . However, as is well known, the equation of state of the dark energy, parameterized by  $w_0$  and  $w_a$ , is poorly constrained by CMB observations alone [47, 48]. This is because the dependence of the CMB power spectrum on these two parameters comes mainly from the distance to last scattering,  $d_{\text{LS}}$ , which involves a double integral of  $w(z)$ :

$$\frac{d_{\text{LS}}}{3000 \text{ Mpc}} \approx \int_0^{z_{\text{rec}}} \frac{dz}{\sqrt{\Omega_m h^2(1+z)^3 + (1-\Omega_m)h^2g(z)}}, \quad (22)$$

where  $z_{\text{rec}}$  is the redshift of recombination, and where

$$g(z) \equiv \exp \left\{ 3 \int_0^z \frac{(1+w(z'))dz'}{1+z'} \right\}. \quad (23)$$

Since  $w_0$  and  $w_a$  only appear inside this double integral, there is a severe degeneracy that can leave  $d_{\text{LS}}$  nearly invariant under changes in these parameters.

Table III summarizes the results for the DUO wide and deep surveys, both from cluster counts ( $dN/dz$ ) and

power spectrum ( $P_c(k)$ ) [58]. This table addresses the issue of the relative merits of survey size versus depth. Starting with the counts, we see that the constraints for the wide and the deep surveys are of the same order, even though the latter yields about 7 times fewer clusters. This is because the deep survey, despite its limited angular coverage, measures a higher fraction of high-redshift clusters. For the power spectrum, however, the constraints are most sensitive to the total number of clusters. Indeed, the errors on most parameters differ by roughly a factor of  $\sqrt{N_{\text{wide}}/N_{\text{deep}}} \approx 2.6$ , where  $N_{\text{wide}}$  and  $N_{\text{deep}}$  are the total number of clusters for the respective surveys. The power spectrum  $P_c(k)$  delivers good constraints on the densities ( $\Omega$ 's) and on  $\sigma_8$  in the wide survey, but has little sensitivity to  $w_0$  and  $w_a$ .

Table IV addresses the issue of the relative merits of  $dN/dz$ ,  $P_c(k)$ , their combination, and their combination with CMB anisotropy data from Planck, for all three surveys. The top third of Table IV lists the results of combining DUO wide and deep. Of particular interest is the third column from the left, which shows the constraints obtained by adding the Fisher matrices for  $dN/dz$  and  $P_c(k)$  for the combined survey. These are, in short, the most optimistic error bars from DUO alone. The table also illustrates the power of combining cluster counts with two-point function statistics. Indeed, the combined error bars (column 3) for  $\Omega_{\text{DE}}$  and  $\Omega_m h^2$  are about two times smaller than those derived from either  $dN/dz$  (column 1) or  $P_c(k)$  (column 2) alone. Finally, we see in the last column that combining DUO and Planck further reduces the uncertainty on  $w_0$  and  $w_a$  by approximately a factor of two. This underscores the complementarity of cluster and CMB data in uncovering the nature of the dark energy.

The middle third of Table IV shows our results for the SPT-like SZE survey. Overall, the constraints on the cosmological parameters are similar to those available from the DUO-like survey.

The bottom third of Table IV shows our estimated parameter uncertainties for the LSST-like cluster survey. Comparing the third column with the previous two again confirms the power of combining counts with power spectrum. The constraints on  $w_0$  and  $w_a$  are of the order of a few percent. These remarkably tight bounds (comparing favorably with those from the Planck survey [Table II] for all cosmological parameters except  $\Omega_m h^2$ ,  $\Omega_b h^2$  and  $n_s$ ) are the result of the very high cluster yield of this survey. To examine the sensitivity of these results to the inclusion of the lowest mass clusters, we follow a more conservative approach by imposing a minimum mass of  $2 \times 10^{14} h^{-1} M_{\odot}$ . This reduces the number of clusters to  $\sim 50,000$ . The constraints on  $w(a)$  from LSST alone degrade by a factor of about two (consistent with  $\sqrt{N}$  scaling of statistical errors), to  $\Delta w_0 = 0.030$  and  $\Delta w_a = 0.23$ . When combined with Planck, the errors are nearly unaffected:  $\Delta w_0 = 0.024$  and  $\Delta w_a = 0.070$ . Therefore we are confident that with enough clusters and combining with Planck, LSST can constrain  $w_a$  to a few

TABLE IV: Estimated Cosmological Parameter Constraints from Clusters and CMB Combined. The  $dN/dz$  column includes priors from WMAP:  $\Delta\Omega_bh^2 = 0.0010$ , and  $\Delta n_s = 0.040$ .

Survey and Parameter Constraints	$dN/dz$	$P_c(k)$	$dN/dz + P_c(k)$	$dN/dz + P_c(k) + \text{Planck}$
<b>DUO Combined</b>				
$\Delta\Omega_{\text{DE}}$	0.011	0.032	0.0074	0.0064
$\Delta\Omega_m h^2$	0.022	0.084	0.0098	0.00041
$\Delta\sigma_8$	0.016	0.088	0.012	0.011
$\Delta w_0$	0.10	0.45	0.096	0.061
$\Delta w_a$	0.48	2.3	0.45	0.19
$\Delta\Omega_bh^2$	0.0010	0.021	0.0010	0.00011
$\Delta n_s$	0.040	0.15	0.033	0.0024
<b>SPT-like Survey (4,000 deg<math>^2</math>)</b>				
$\Delta\Omega_{\text{DE}}$	0.036	0.033	0.014	0.0097
$\Delta\Omega_m h^2$	0.049	0.056	0.0083	0.00027
$\Delta\sigma_8$	0.031	0.064	0.018	0.012
$\Delta w_0$	0.22	0.41	0.15	0.082
$\Delta w_a$	0.59	1.8	0.46	0.18
$\Delta\Omega_bh^2$	0.0010	0.014	0.00099	0.00011
$\Delta n_s$	0.040	0.094	0.029	0.0023
<b>LSST-like Survey (18,000 deg<math>^2</math>)</b>				
$\Delta\Omega_{\text{DE}}$	0.0053	0.0080	0.0024	0.0023
$\Delta\Omega_m h^2$	0.026	0.021	0.0048	0.00024
$\Delta\sigma_8$	0.0035	0.022	0.0025	0.0024
$\Delta w_0$	0.051	0.10	0.024	0.023
$\Delta w_a$	0.086	0.47	0.077	0.061
$\Delta\Omega_bh^2$	0.0010	0.0050	0.00097	0.00010
$\Delta n_s$	0.040	0.040	0.015	0.0022

percent. Finally, we find that it is essential to include the cosmology-dependence of the limiting mass for the LSST survey. Repeating our analysis adopting the redshift-dependent mass limit from the fiducial cosmology, and not allowing it to vary with cosmology, results in an increase by a factor of 3–4 in the uncertainties.

In Table V, we repeat the analysis for the DUO and SPT-like surveys, but this time taking into account the uncertainty in the structure and evolution of clusters. In other words, we require that the cluster surveys constrain not only the cosmology, but also the parameters of the mass-observable relation. For DUO, this is modeled by including the parameters  $A_x$ ,  $\beta_x$  and  $\gamma_x$  of Eq. (17) in the Fisher matrix analysis. Similarly, for the SPT-like survey, we include  $A_{sz}$ ,  $\beta_{sz}$  and  $\gamma_{sz}$  from Eq. (18). For both surveys, we see that adding self-calibration increases the error on  $w_0$  and  $w_a$  by a factor of  $\lesssim 2$  in comparison with the corresponding results in Table IV. Overall, we see that including self-calibration parameters still yields very good constraints on the cosmology. The constraints from  $dN/dz + P_c(k)$  and  $dN/dz + P_c(k) + \text{Planck}$  are shown graphically in Figs. 2 and 3, including self-calibration for the DUO-like and SPT-like surveys.

Coming back to Table IV and comparing the first column from the left ( $dN/dz$ ) with the third ( $dN/dz +$

$P_c(k)$ ), we note that, for DUO, adding the power spectrum does not significantly tighten the constraints on  $w_0$  and  $w_a$  in this case. However, for the “self-calibration” case (Table V), combining the two methods helps greatly on all the constraints. For SPT-like and LSST-like surveys, combining two methods always gives stronger constraints. This is clearly illustrated in Fig. 2.

An obvious method to cross-check for systematic effects due to cluster structure and evolution, and to improve constraints, is to combine the X-ray and SZE data. We have found that the uncertainties in  $w_0$  and  $w_a$  reduce to 0.083 and 0.35 when the self-calibrated SPT and DUO samples are considered in combination, and to 0.060 and 0.22 when Planck is added to this combined sample.

Uncertainties in cluster structure and evolution should be less severe for WL signatures, which probe the dark matter potential directly. However, to compare the WL error forecasts more fairly with the SZ and X-ray predictions, in Table VI we show LSST predictions that incorporate two additional uncertainties inherent to WL selection: false detections and incompleteness. We relied on published results of numerical simulations [41, 42] to calibrate our results: we assumed 25% of detections are false, and 30% of real clusters are undetected. These effects increase the parameter errors, relative to those in

TABLE V: Parameter Constraints including Self-Calibration. The  $dN/dz$  column includes priors from WMAP:  $\Delta\Omega_bh^2 = 0.0010$ , and  $\Delta n_s = 0.040$ .

Survey and Parameter Constraints	$dN/dz$	$P_c(k)$	$dN/dz + P_c(k)$	$dN/dz + P_c(k) + \text{Planck}$
<b>DUO Combined</b>				
$\Delta\Omega_{\text{DE}}$	0.030	0.043	0.015	0.012
$\Delta\Omega_m h^2$	0.14	0.091	0.0098	0.00067
$\Delta\sigma_8$	0.058	0.12	0.016	0.013
$\Delta w_0$	0.44	0.53	0.20	0.15
$\Delta w_a$	1.2	2.5	0.82	0.46
$\Delta\Omega_b h^2$	0.0010	0.022	0.0010	0.00011
$\Delta n_s$	0.040	0.18	0.034	0.0027
$\Delta \log A_x$	0.27	0.18	0.050	0.037
$\Delta b_x$	0.29	0.18	0.030	0.027
$\Delta\gamma_x$	0.67	0.63	0.17	0.081
<b>SPT-like survey</b>				
$\Delta\Omega_{\text{DE}}$	0.13	0.037	0.017	0.014
$\Delta\Omega_m h^2$	0.65	0.077	0.0086	0.00063
$\Delta\sigma_8$	0.14	0.099	0.019	0.017
$\Delta w_0$	0.42	0.46	0.19	0.14
$\Delta w_a$	2.4	1.8	0.81	0.40
$\Delta\Omega_b h^2$	0.0010	0.018	0.0010	0.00011
$\Delta n_s$	0.040	0.15	0.032	0.0026
$\Delta \log A_{sz}$	0.59	0.35	0.12	0.056
$\Delta b_{sz}$	0.79	0.35	0.12	0.063
$\Delta\gamma_{sz}$	1.7	0.62	0.19	0.057

TABLE VI: Calibrated Cosmological Parameter Constraints from LSST and CMB Combined. The  $dN/dz$  column includes priors from WMAP:  $\Delta\Omega_bh^2 = 0.0010$ , and  $\Delta n_s = 0.040$ .

Parameter Constraints	$dN/dz$	$P_c(k)$	$dN/dz + P_c(k)$	$dN/dz + P_c(k) + \text{Planck}$
<b>LSST-like Survey</b>				
$\Delta\Omega_{\text{DE}}$	0.0081	0.012	0.0037	0.0033
$\Delta\Omega_m h^2$	0.038	0.032	0.0059	0.00024
$\Delta\sigma_8$	0.0054	0.034	0.0038	0.0037
$\Delta w_0$	0.079	0.16	0.037	0.036
$\Delta w_a$	0.13	0.72	0.12	0.093
$\Delta\Omega_b h^2$	0.0010	0.0077	0.00098	0.00010
$\Delta n_s$	0.040	0.062	0.021	0.0022

the bottom third of Table IV by  $\approx 50\%$  (except for  $\Omega_bh^2$  and  $n_s$ , which are significantly determined by the WMAP priors and are less affected). See the next section for a more detailed discussion.

#### IV. DISCUSSION

In the previous section, we derived constraints on cosmological parameters from future SZE, X-ray, and WL surveys. Our Fisher matrix approach should be interpreted as yielding lower limits on the achievable statistical errors. In our analysis, we adopted unique relations between the observables and cluster mass, which come

from simple models of cluster structure and evolution. We required the SZ and X-ray surveys to “self-calibrate” and constrain structure and evolution parameters simultaneously with cosmology. However, the power-law form of the relations we adopted will have to be further constrained. This should be feasible by combining the three observables in the different wave bands for a subset of the samples, and by adding new observables (such as the shape of the mass function, the angular size, velocity dispersion) which we have not considered here. In the case of the WL sample, we relied on results from numerical simulations to calibrate the mass-observable relation, an approach that can be refined with a larger suite of simulations in the future.

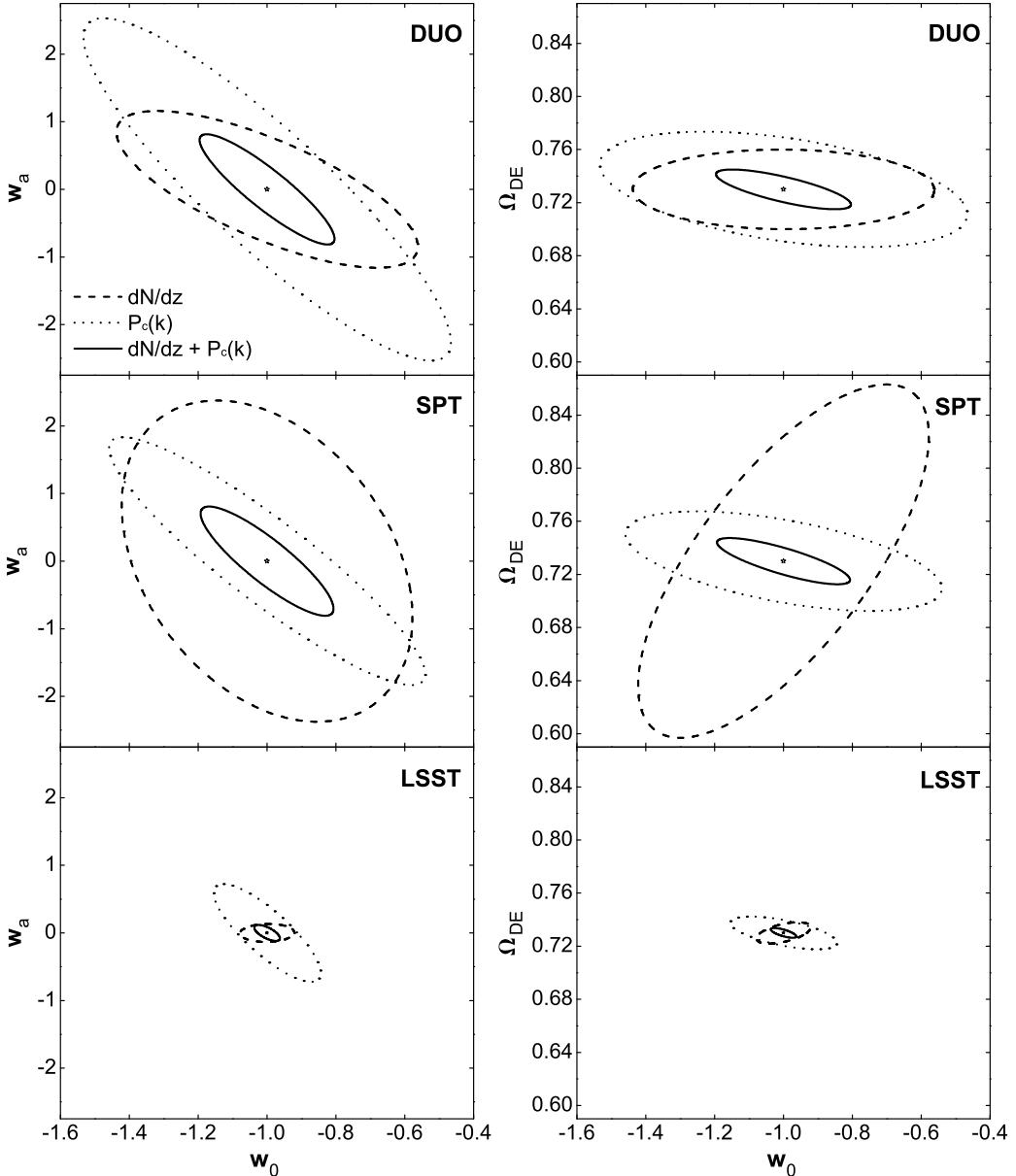


FIG. 2: Constraints on dark energy parameters:  $w_0$  and  $w_a$  (left),  $w_0$  and  $\Omega_{\text{DE}}$  (right) for a DUO-like X-ray survey (top), an SPT-like SZE survey (middle), and an LSST-like weak lensing survey (bottom). The three curves in each figure show the constraints available from  $dN/dz$  (dashed),  $P_c(k)$  (dotted), and from their combination (solid). The star-shaped symbol at the center of each figure indicates our fiducial cosmology. The constraints for X-ray survey and SZE survey are calculated for the self-calibration case. The constraints are marginalized over all other cosmological and relevant structure parameters. In all cases, the constraints from the combination of  $dN/dz$  and  $P_c(k)$  are at least a factor of two stronger than from either method alone.

The Fisher matrix technique, especially the way of combining independent constraints by summing individual Fisher matrices, allows us to explore the physical origin of the cosmological information. A glance at Eqs. (8) and (10) reveals that cosmology enters through several physical quantities into the Fisher matrices, such as the cosmic volume, growth function, transfer function, bias, etc. Unfortunately, the marginalization over all other

parameters involves a nonlinear inversion of the Fisher matrix, which makes isolating the various sources of information difficult. As an example, we repeated the analysis above, but keeping either the volume factor,  $k_\perp^2 k_\parallel$ , or the bias parameter at their values in the fiducial model (*i.e.*, excluding their derivatives from computing power spectrum Fisher matrices). We find that as a result, the constraint on some of the parameters improve, while oth-

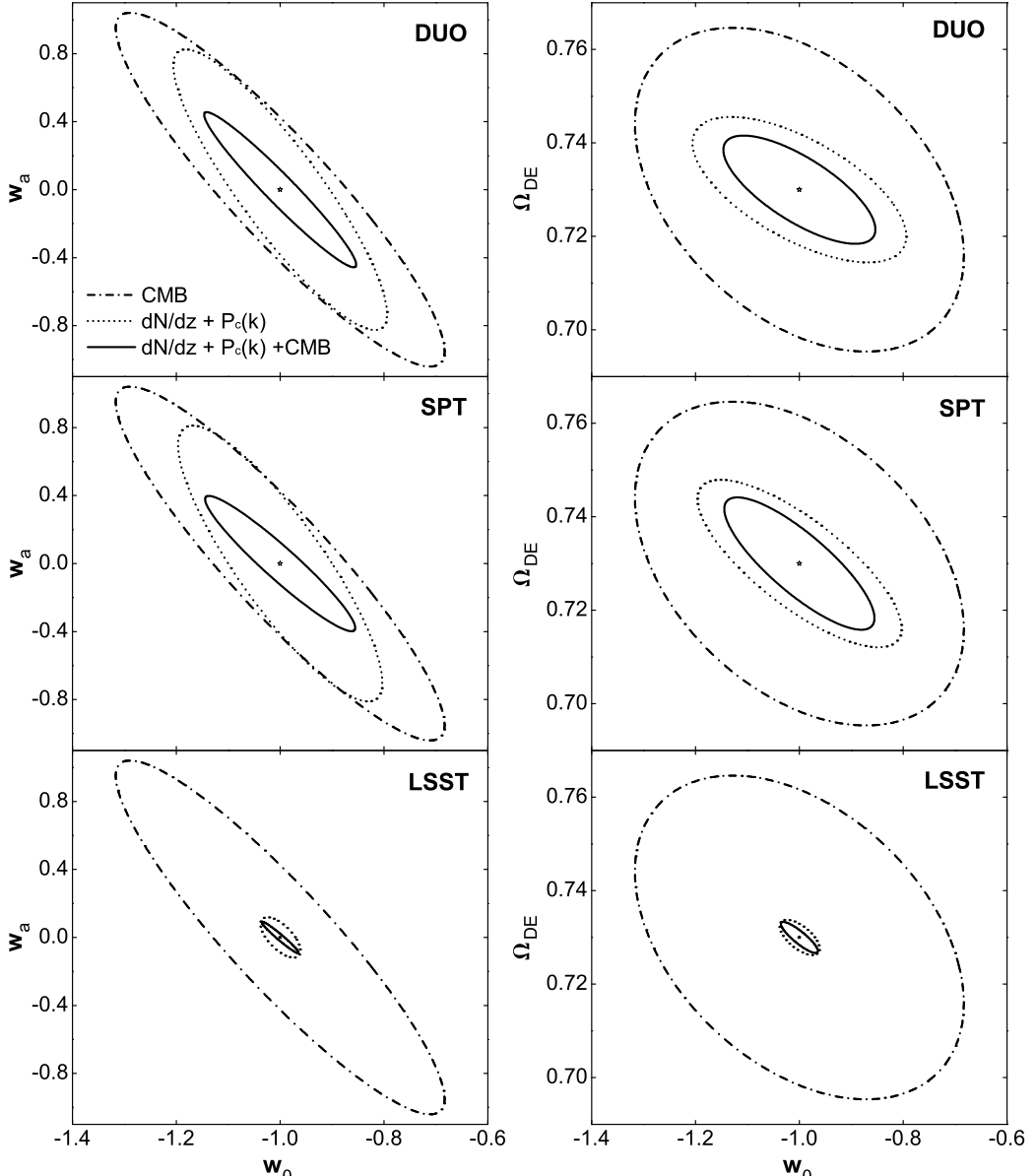


FIG. 3: Constraints on dark energy parameters:  $w_0$  and  $w_a$  (left),  $w_0$  and  $\Omega_{\text{DE}}$  (right), by combining a DUO-like X-ray survey (top), an SPT-like SZE survey (middle), or an LSST-like weak lensing survey (bottom) with Planck-like CMB observations. The three curves in each figure show the constraints available from the combination of  $dN/dz$  and  $P_c(k)$  (dotted), CMB alone (dot-dashed), and from the combination of all of the above (solid). As in Fig. 2, the constraints for X-ray survey and SZE surveys are calculated for the self-calibration case, and constraints are marginalized over all other relevant parameters. Note the different scales of the horizontal and vertical axes compared to Fig. 2.

ers degrade, which does not offer a useful description of the amount of information the volume factor or the bias parameter provides.

In addition, we explored the implicit assumption made above that the bias parameter  $b$  can be precisely modeled. We take a similar approach to that used in addressing “self-calibration”, by modeling the bias as  $b = b_0(z)(1+z)^{\gamma_b}$ . We effectively include an additional new parameter,  $\gamma_b$ , in the Fisher matrix analysis. Note that a constant

factor of normalization would be degenerate with  $\sigma_8$ . In the fiducial model,  $b_0(z)$  follows from Eq. (5), and  $\gamma_b = 0$ . The constraints from cluster power spectrum including the “non-standard evolution parameter”  $\gamma_b$  causes only a minor degradation (under 10%) of the constraints on  $w_0$  and  $w_a$  (relative to column 2 in Table IV), suggesting that the bias factor did not drive the cosmological constraints we derived from the power spectrum.

The results from the power spectrum also depend on

the assumption of the extent of the linear regime. To quantify the importance of the small-scale modes, for the example of the SPT-like survey, we decreased  $k_{\max}$  from 0.15 to 0.10  $\text{Mpc}^{-1}$ . We found that this degrades the error bars by a factor of up to  $\approx 1.4$ . Similarly, decreasing  $k_{\max}$  further to 0.075  $\text{Mpc}^{-1}$  degrades all the error bars by a factor of up to  $\approx 2$ . (See also [14] for a detailed discussion of the dependence of the constraints separately on  $k_{\perp,\max}$  and  $k_{\parallel,\max}$ .)

In Table IV, we have assumed that the mass-observable relations apply exactly. However, for real surveys, the mass-observable relation is likely to have a non-negligible scatter. We estimated the magnitude of scatter that would bias the inferred parameters by an amount comparable to their statistical errors, for the example of the SPT survey [27]. We assumed that at a fixed flux  $f_{sz}$ , the mass  $M_{180}$  has a Gaussian distribution, with a mean given by Eq. 18 (but converted from  $M_{200}$  to  $M_{180}$ ), and a fractional r.m.s. deviation of  $\delta M/M = \sigma_M$ . We then re-computed the cluster abundance  $dN/dz$  (which is increased in the presence of scatter). We found that at  $\sigma_M \approx 7\%$ , the change caused in the total number of detectable clusters is comparable to the  $\sqrt{N}$  error that is used to obtain the constraints on cosmological parameters. A scatter larger than  $\sim 7\%$  would therefore be important, and it would have to be modeled (i.e. by parameterizing the scatter, calibrated directly from observations) in the analysis of real data.

A further complication, likely most relevant for the WL survey, is the presence of false detections. In our analysis of the LSST-like survey, we used a constant shear S/N to select clusters, which directly measures how well the shear signal stands out above the ellipticity shot noise of the background galaxies. False detections can result from statistical fluctuations in these ellipticities. Furthermore, physical structures, projected along the line of sight to a given cluster, constitute additional background noise, and can result in a false detection of two or more mass concentrations (projected along the line of sight but physically separated in redshift). Hennawi & Spergel [42] have done a comprehensive study of mass-selected clusters using  $N$ -body simulations (see also [41, 49] for other numerical studies of WL cluster selection). Defining *efficiency* as the fraction of the peaks in the mass map that corresponds to real clusters, and *completeness* as the fraction of real clusters we can detect, they find in their simulation that for a 4.5 standard deviation detection threshold,  $\approx 75\%$  of the detected clusters are real and  $\approx 70\%$  of the clusters can be detected [41]. They emphasize that the expected cluster distribution, including false detections and missing clusters, can be reliably calculated for any cosmological model since the simulations depend only on gravity. Thus, false detections can be subtracted, and their presence serves only to increase the statistical error. These effects would increase the parameter errors in the bottom third of Table IV by  $\approx 50\%$  (summing in quadrature the errors on the number of real clusters and on the number of false-detections,

$\sqrt{((1/e - 1) + 1/e)/c} - 1 \approx 50\%$ , where  $e = 75\%$  is the efficiency and  $c = 70\%$  is the completeness as we defined above).

We note that the study in [42] utilized only the ‘‘tomographic redshifts’’ derived from the shear map itself (using photometric redshifts only for the background galaxies), which have large uncertainties. However, it should be feasible to routinely measure photometric redshifts of the cluster member galaxies, as well, and this additional information could be used to reduce the rate of false detections.

Obtaining redshifts is a general issue relevant for all three future surveys. While accurate (spectroscopic) redshifts are not required for either the  $dN/dz$  or  $P(k)$  tests, photometric redshift estimates will be required to utilize the distribution of clusters in  $z$ , and also to use high- $k_{\parallel}$  modes of the power spectrum. In the case of the LSST survey, we adopted a maximum redshift  $z_{\max} = 1.4$ , the redshift out to which it should be feasible to obtain photometric redshifts with the planned filters and sensitivities [25]. In the case of DUO, most of the clusters in the wide survey ( $\gtrsim 80\%$ ) will have photometric redshifts from the overlapping Sloan Digital Sky Survey (SDSS) galaxies; the redshifts of the more distant galaxies in the deep survey will be obtained in optical follow-up programs. Obtaining photometric redshifts of a large fraction of clusters in the SPT survey beyond  $z \gtrsim 1.4$  will be challenging. However, we have re-computed our results for SPT ignoring all clusters beyond  $z = 1.4$ , and found that none of the constraints degraded by more than a few percent.

It has often been argued that weak lensing only involves gravitational deflection of light, so the mass-shear relation can be determined without fully understanding the complex baryonic physics. Clearly this is an idealization, since baryons can cool and contract to establish a more centrally-condensed density profile than the dark matter, altering the total gravitational field. To quantify the resulting change in the WL shear, we followed a simple spherical model in [50], in which a fixed fraction  $f_{\text{cool}}$  of baryons inside a ‘cooling radius’ are allowed to cool and condense by a further factor of  $\sim 10$  after virialization. The effect of such a ‘cooling flow’ on the mass profiles of halos is relatively small, except in the inner regions. In models with  $f_{\text{cool}}$  up to 30 %, we find that the change in the Gaussian-averaged shear  $\kappa_G$  can be up to 15%. This reflects the enhanced effect of baryons in the core of the cluster, which is emphasized by the Gaussian weighting. However, this bias only affects the initial selection of clusters. In practice, one will go back and extract the total mass of the cluster from the shear map in a separate analysis [51]. We find that the total mass enclosed within the virial radius is changed by a much smaller amount,  $< 1\%$ .

In this work, the constraints on cosmological parameters were derived assuming a fiducial model with a cosmological constant as the dark energy, *i.e.*,  $w_0 = -1$  and  $w_a = 0$ . As mentioned above, the choice of the fiducial

model can, in principle, strongly affect the predicted errors. To assess the robustness of our derived errors, we repeated the analysis for a fiducial model with a strongly time-dependent equation of state, namely  $w_0 = -0.8$  and  $w_a = 0.3$ , which is also consistent with current data. We find in this case that all error bars derived from  $dN/dz$  and  $P(k)$  remain essentially unchanged, except for  $\Delta w_a$ , which shrinks by about 25%. Therefore, by choosing a pure  $\Lambda$  model as our fiducial cosmology, we obtain a conservative estimate of the error on  $w_a$ .

## V. CONCLUSIONS

Three main lessons can be drawn from our work. First, the above results provide further support for the usefulness of clusters as an independent and important probe of the dark energy. At a general level, the main advantage of clusters over other measurements lies in the fact that the physics involved is predominantly gravitational and hence simple; moreover, the observations are at low redshift and therefore straddle the epoch of cosmic acceleration.

We have seen that even cluster counts ( $dN/dz$ ) alone can yield comparable or even better constraints on  $w_0$  and  $w_a$  than a full-sky, high-precision CMB survey such as Planck. Our constraints are summarized in Table IV. Of course, this assumes perfect knowledge of the mass-observable relation, *i.e.*, that the clusters are standard candles. We have shown, however, that even after allowing for uncertainty in cluster evolution and structure, and using the survey itself as a calibration tool, the errors on  $w_0$  and  $w_a$  still compare respectably well with Planck, as seen from the third column of Table V. The constraints from cluster surveys also compare favorably with other cosmological probes. For instance, current constraints from type Ia supernovae are on the order of  $\Delta w_0 \approx 0.3$  and  $\Delta w_a \approx 1.6$  [52], assuming a strong prior of  $\Delta \Omega_m = 0.04$  from other measurements. The expected errors from the *Supernovae Acceleration Probe* (SNAP) are  $\Delta w_0 \approx 0.08$  and  $\Delta w_a \approx 0.3$ , with the same prior on  $\Omega_m$  [53]. Relaxing this prior results in errors on the order of  $\Delta w_0 \approx 0.2$  and  $\Delta w_a \approx 1.0$  [47], comparable to our projected constraints from DUO or SPT.

A second lesson we wish to draw is the power of com-

bining different cluster observables in constraining cosmological parameters, in this case cluster counts ( $dN/dz$ ) and two-point statistics ( $P_c(k)$ ). The most striking illustrations of this are the LSST-like survey (see Table IV) where  $\Delta w_0$  is a factor of  $\sim 2$  smaller after combining the two methods; and the SPT-like self-calibrated case (see Table V) where both  $\Delta w_0$  and  $\Delta w_a$  shrink by a factor of  $\gtrsim 2$ . While we have focused here on  $dN/dz$  and  $P_c(k)$ , other cluster observables that could be included are three-point correlation functions, assuming a large enough survey, information from the shape of the mass function,  $dN/dM$ , as described in [11], or scaling relations [54]. We leave a more comprehensive study of such additional cluster observables for future work.

Finally, our work underscores the complementarity of cluster observables to CMB anisotropy. In general, we have seen that adding the information from a Planck-like survey reduces  $\Delta w_0$  and  $\Delta w_a$  by a factor of 2 or so (although the LSST-like WL survey has already very small errors, and adding Planck data improves the constraints by a more modest amount). Thus clusters not only constitute a powerful cosmological probe in their own right, but also help in alleviating CMB observations from some of their well-known degeneracies.

Future work includes the addition of other cluster observables, as mentioned earlier, as well as using cluster surveys to place useful constraints on the neutrino mass [55].

## Acknowledgments

We thank Joseph Hennawi, Wayne Hu, Joseph Mohr, and the members of the DUO team for insightful discussions, Jochen Weller for useful comments on the manuscript, Gil Holder and Joseph Mohr for useful comments on SPT's sensitivity, Subhabrata Majumdar for assistance in cross-checking our numerical codes, Pier-Stefano Corasaniti for allowing us to use his modified version of CMBFAST, and an anonymous referee whose comments improved this paper. This work is supported in part by the US Department of Energy under Contract No. DE-AC02-98CH10886, by the Columbia University Academic Quality Fund and the Ohrstrom Foundation (JK).

---

[1] P.T.P. Viana and A.R. Liddle, MNRAS **281**, 323 (1996).  
[2] S.D.M. White, G. Efstathiou and C.S. Frenk, MNRAS **262**, 1023 (1993).  
[3] N.A. Bahcall and X. Fan, Astrophys. J. **504**, 1 (1998).  
[4] A. Blanchard and J.G. Bartlett, Astron. Astrophys. **332**, L49 (1998).  
[5] P.T.P. Viana and A.R. Liddle, MNRAS **303**, 535 (1999).  
[6] L. Wang and P.J. Steinhardt, Astrophys. J. **508**, 483 (1998).  
[7] Z. Haiman, J.J. Mohr and G.P. Holder, Astrophys. J. **553**, 545 (2001).  
[8] G.P. Holder, Z. Haiman and J.J. Mohr, Astrophys. J. **560**, L111 (2001).  
[9] W. Hu and A.V. Kravtsov, Astrophys. J. **584**, 702 (2003).  
[10] E.S. Levine, A.E. Schultz and M. White, Astrophys. J. **577**, 569 (2002).  
[11] W. Hu, Phys. Rev. D **67**, 081304 (2003).  
[12] J. Weller, R.A. Battye and R. Kneissl, Phys. Rev. Lett. **88**, 1301 (2002).

- [13] J. Weller and R.A. Battye, *New Astronomy Reviews* **47**, 775 (2003).
- [14] W. Hu and Z. Haiman, *Phys. Rev. D* **68**, 3004 (2003).
- [15] T. Matsubara and A.S. Szalay, *Astrophys. J.* **574**, 1 (2002).
- [16] A. Refregier, I. Valtchanov and M. Pierre, *A&A* **390**, 1 (2002).
- [17] C. Blake and K. Glazebrook, *Astrophys. J.* **594** 665 (2003).
- [18] H.-J. Seo and D.J. Eisenstein, *Astrophys. J.* **598**, 720 (2003).
- [19] E.V. Linder, *Phys. Rev. D* **68**, 3504 (2003).
- [20] P. Schuecker, H. Böhringer, C.A. Collins and L. Guzzo, *A&A* **398**, 867 (2003).
- [21] S. Majumdar and J.J. Mohr, *Astrophys. J.*, submitted, [astro-ph/0305341](http://astro-ph/0305341).
- [22] S. Majumdar and J.J. Mohr, *Astrophys. J.* **585**, 603 (2003).
- [23] See, K. Jahoda, *Astronomische Nachrichten* **324**, 132 (2003) for description of a similar, previously proposed survey, DUET.
- [24] J.E. Ruhl, *et al.*, Proc. SPIE, vol. 5498, p. 11 (2004), [astro-ph/0411122](http://astro-ph/0411122); See also [astro.uchicago.edu/spt](http://astro.uchicago.edu/spt).
- [25] See, [www.lsst.org](http://www.lsst.org).
- [26] A. Jenkins *et al.*, *MNRAS* **321**, 372 (2001).
- [27] R.A. Battye and J. Weller, *Phys. Rev. D* **68**, 083506 (2003).
- [28] J.F. Navarro, C.S. Frenk and S.D.M. White, *Astrophys. J.* **490**, 493 (1997).
- [29] N. Kaiser, *MNRAS* **227**, 1 (1987).
- [30] R.K. Sheth and G. Tormen, *MNRAS* **308**, 119 (1999).
- [31] M. Tegmark, A.N. Taylor and A.F. Heavens, *Astrophys. J.* **480**, 22 (1997).
- [32] H.A. Feldman, N. Kaiser and J.A. Peacock, *Astrophys. J.* **426**, 23 (1994).
- [33] See, [www.rssd.esa.int/index.php?project=PLANCK](http://www.rssd.esa.int/index.php?project=PLANCK).
- [34] M. Zaldarriaga and U. Seljak, *Phys. Rev. D* **55**, 1830 (1997).
- [35] M. Zaldarriaga, D.N. Spergel and U. Seljak, *Astrophys. J.* **488**, 1 (1997).
- [36] See, *e.g.*, G. Rocha *et al.*, *MNRAS*, submitted, [astro-ph/0309211](http://astro-ph/0309211).
- [37] P.S. Corasaniti, M. Kunz, D. Parkinson, E.J. Copeland and B.A. Bassett, *Phys. Rev. D* **70**, 083006 (2004).
- [38] U. Seljak and M. Zaldarriaga, *Astrophys. J.* **469**, 437 (1996); see also [www.cmbfast.org](http://www.cmbfast.org).
- [39] D.N. Spergel *et al.*, *Astrophys. J. Suppl.* **148**, 175 (2003).
- [40] I.M. Gioia *et al.*, *Astrophys. J.* **553**, L105 (2001).
- [41] T. Hamana, M. Takada and N. Yoshida, accepted by MNRAS, [astro-ph/0310607](http://astro-ph/0310607).
- [42] J.F. Hennawi and D.N. Spergel, *Astrophys. J.*, submitted, [astro-ph/0404349](http://astro-ph/0404349).
- [43] L. Van Waerbeke, *MNRAS* **313**, 524 (2000).
- [44] Y.-S. Song and L. Knox, *Phys. Rev. D*, submitted, [astro-ph/0312175](http://astro-ph/0312175).
- [45] D.J. Eisenstein, W. Hu and M. Tegmark, *Astrophys. J.* **518**, 2 (1998).
- [46] W. Hu, *Phys. Rev. D* **65**, 023003 (2002).
- [47] I. Maor, R. Brustein and P.J. Steinhardt, *Phys. Rev. Lett.* **86**, 6 (2001); *Erratum-ibid* **87**, 049901 (2001); I. Maor, R. Brustein, J. McMahon and P.J. Steinhardt, *Phys. Rev. D* **65**, 123003 (2001).
- [48] J.A. Frieman, D. Huterer, E.V. Linder and M.S. Turner, *Phys. Rev. D* **67**, 083505 (2003).
- [49] M. White, L. van Waerbeke and J. Mackey, *Astrophys. J.* **575**, 640 (2002).
- [50] M. White, accepted by *Astroparticle Phys.*, [astro-ph/0405593](http://astro-ph/0405593).
- [51] G. Fahlman, N. Kaiser, G. Squires and D. Woods, *Astrophys. J.* **437**, 56 (1994).
- [52] A.G. Reiss *et al.*, accepted by *Astrophys. J.*, [astro-ph/0402512](http://astro-ph/0402512).
- [53] See, [snap.lbl.gov](http://snap.lbl.gov).
- [54] L. Verde, Z. Haiman and D.N. Spergel, *Astrophys. J.* **581**, 5 (2002).
- [55] S. Wang, Z. Haiman, W. Hu, J. Khouri and M. May, in preparation.
- [56] Note that we use the fitting formula describing the unsmoothed mass function in the simulations, given in Eq. (B3) in Jenkins *et al.* [26], which is more appropriate to galaxy clusters than the smoothed mass function [9].
- [57] It has been pointed out [27] that clusters are extended sources, and a convolution with SPT's beam profile leads to a loss of sensitivity. This reduces in [27] the number of clusters detectable with SPT to  $\sim 4500$ . However, this reduction stems from the *point source* sensitivity of 5 mJy adopted in [27]. The threshold of 5 mJy we chose represents the *total flux* of an extended cluster, and it can be roughly understood as follows. The sensitivity of SPT at 150 GHz within its 1 square arcminute beam is  $\sim 10 \mu\text{K}$  [24], corresponding to 0.3 mJy. The  $\sim 2$  arcmin inner region of the smallest detectable cluster fills  $\sim 12$  beams, yielding a total noise of  $\sim 1$  mJy within the cluster aperture.
- [58] In this Table, as well as in Tables IV and V below, we have included priors on  $\Omega_b h^2$  and  $n_s$  from the present constraints on these parameters from WMAP (0.001 and 0.04, respectively) for the  $dN/dz$  Fisher matrix. The motivation of adding these priors is that  $dN/dz$  has essentially no sensitivity to these two parameters, resulting in large predicted uncertainties which obscure the information content of  $dN/dz$ . The  $dN/dz$  and  $dN/dz + P(k)$  columns in all three tables reflect these WMAP priors. In the last column, when CMB information from Planck is added in Tables IV and V below, the WMAP priors become irrelevant.